

A Single GPS Receiver as a Real-Time, Accurate Velocity and Acceleration Sensor

Luis Serrano, Don Kim and Richard B. Langley
*Department of Geodesy and Geomatics Engineering
University of New Brunswick, Canada*

BIOGRAPHIES

Luis Serrano obtained his diploma in geographic engineering from the Faculty of Sciences of the University of Lisbon, Portugal. For 4 years he worked as a geodetic engineer in private companies. Currently he is a Ph.D. student in the Department of Geodesy and Geomatics Engineering at the University of New Brunswick, where he carries out research in real-time precise navigation in indoor/outdoor environments.

Don Kim is a research associate in the Department of Geodesy and Geomatics Engineering at the University of New Brunswick, where he has developed the UNB RTK software for a gantry crane auto-steering system. He has a B.Sc., M.Sc. and Ph.D. in geomatics from Seoul National University. He has been involved in GPS research since 1991. Currently, Dr. Kim carries out research related to ultrahigh-performance RTK positioning at up to a 50 Hz data rate, with application to real-time deformation monitoring, Internet-based moving platform tracking, and machine control.

Richard B. Langley is a professor in the Department of Geodesy and Geomatics Engineering at the University of New Brunswick, where he has been teaching and conducting research since 1981. He has a B.Sc. in applied physics from the University of Waterloo and a Ph.D. in experimental space science from York University, Toronto. Professor Langley has been active in the development of GPS error models since the early 1980s and is a contributing editor and columnist for GPS World magazine.

ABSTRACT

The determination of velocity and acceleration from GPS measurements is very important for many dynamic applications, but also for airborne gravimetry and geophysics, as long as we can achieve the specific accuracy and resolution for each application. The use of GPS receivers rather than speedometers and/or

accelerometers, is a very attractive option, since they can be more cost-effective, easier to operate and maintain and also they can provide a long-term stable reference.

The estimation of velocity and acceleration from discrete-time signals in GPS is based on the differentiation of the carrier-phase measurements or the receiver-generated Doppler measurements. As with velocity estimation, it is preferable to generate the acceleration measurements from the differentiation of the carrier-phase rather than from the instantaneous Doppler measurement (which is noisier), where for the velocity we obtain range rates and for the acceleration we obtain range accelerations.

The optimal design of a differentiator is the key point for accurate velocity and acceleration estimation from the carrier-phase measurements, which should be a compromise between the noise level reduction, thus the accuracy that can be achievable, but also the spectral resolution of the differentiated signal (bandwidth), because the differentiation method may alias the platform dynamics information contained in the resulting signal. Since this choice depends on the particular platform dynamics, we have investigated different test scenarios and platforms in real-time environments.

To estimate user velocities and accelerations in the range domain, first we need to calculate the satellite velocities and accelerations, where in real time they can be obtained from the broadcast ephemerides with an analytical differentiation of the position parameter equations. The applicability and accuracy of this method usually is not mentioned in publications, since in most cases a post-processing scheme is a preferred approach using precise ephemerides and DGPS precise positions. In this work, we evaluated the effect of the prediction of satellite velocities and accelerations from broadcast ephemerides in determining the user acceleration, but also we developed an error budget for the estimation of velocity and acceleration using a single, autonomous GPS receiver navigating in real time.

INTRODUCTION

Until very recently, GNSS user accelerations were derived from precise DGPS positions. This approach is accordingly called the position method. However, this method requires excellent and continuous positioning accuracies, which may not be achievable under operational conditions [Kennedy, 2002].

Previous work on deriving accelerations from carrier-phase measurements was carried out by Kleusberg et al. [1990], Peyton [1990] and Jekeli [1994], though these results only referred to static results in the acceleration domain. Jekeli and Garcia [1997] continued the work in this field and presented results of kinematic accelerations. Kennedy [2002] presented the most extensive and promising results for kinematic acceleration, but in the gravity domain, which required very precise kinematic acceleration estimates using post-processing schemes and between-receiver differencing. This paper might be considered an extension of this recent work, since we were interested in creating software for evaluating the accuracy of kinematic velocities and accelerations derived from the carrier-phase, though using a stand-alone GPS receiver.

The novelty of this work lies in the fact that we use broadcast ephemerides to calculate the satellite velocities and accelerations (the main contributions to the error budget), and a stand-alone GPS receiver

One of the main advantages of our method is that user positioning accuracy can be relaxed to the order of meters (~10m), which is normally achievable for real-time point-positioning purposes. Thus, motivated by preliminary results coming from this real-time dynamic information, i.e. kinematic velocities and accelerations derived from the carrier-phase method, we wanted to determine if it is possible to improve the real-time position estimates, using an extended Kalman filter (EKF), integrating the kinematic velocities and accelerations in a loosely coupled Kalman filter.

This method to derive accelerations from GNSS measurements is very interesting because the accelerations are already in the navigation frame, thus we do not need sensors like gyroscopes to convert them from the body frame to the navigation frame. The trade-off is that the acceleration components have a latency of one sample interval from the velocities and two from the positions, due to the process of differentiation, though in ultra-performance navigation using up to a 50 Hz data rate, this drawback is eliminated.

Thus, the purpose of this paper is to describe our technique for obtaining real-time precise position, velocity and acceleration solutions using a stand-alone

GPS receiver (Fig. 1), which makes it a very attractive option in many applications, due to many reasons such as simplicity, low maintenance and hence, cost-effectiveness. Furthermore, the velocity and acceleration algorithms described in the following sections can be implemented on different platforms, coupled with different GNSS or INS sensors as necessary.



Figure 1: Platform for the kinematic test.

KINEMATIC VELOCITY AND ACCELERATION

Previous studies on GPS velocity determination show that it is possible to achieve accuracies of a few millimetres per second depending on receiver quality, whether in static or kinematic mode, stand-alone or relative mode, and the particular dynamics situation [Van Graas and Soloviev, 2003; Ryan et al., 1997].

The velocity of the receiver mounted on a moving platform can be determined by using carrier-phase-derived Doppler measurements or receiver-generated Doppler measurements.

A receiver-generated Doppler measurement is a measure of near instantaneous velocity, whereas the carrier-phase-derived Doppler is a measure of mean velocity between observation epochs. The direct Doppler measurement is noisier than carrier-phase-derived Doppler because it is determined over a very small time interval. As carrier-phase-derived Doppler is computed over a longer time span, the random noise is averaged and lowered. Therefore, very smooth velocity is obtained by carrier-

phase-derived Doppler observation if there are no undetected cycle slips.

The carrier-phase-derived Doppler can be obtained by either differencing carrier-phase observations in the time domain, normalizing them with the time interval of the differenced observations or by fitting a curve to successive phase measurements (delta-ranges), using polynomials of various orders.

Extending this differencing approach in the measurement domain, it is also possible to estimate GPS based-kinematic accelerations, determined by differentiating range rates with respect to time to determine line of sight range accelerations. Actually, one is differentiating twice in succession the raw carrier-phase measurements, to obtain the range accelerations.

DIFFERENTIATORS (FIR FILTER)

The ideal digital differentiator can be written in the following form:

$$H(e^{j\omega T}) = j\omega \quad \text{for } 0 \leq |\omega| \leq \frac{\omega_s}{2} \quad (1)$$

where H is the differentiator, ω is the frequency, ω_s is the sampling frequency and T is the corresponding sampling period. To differentiate a discrete time signal, such as GPS data, one can use a discrete time convolution, or in other words, the differentiator can be considered as a non-recursive or finite impulse response (FIR) filter. Practically, a FIR differentiator can be applied to a discrete data set, such as the L1 carrier-phase time series $\Phi(t)$, using a convolution as follows:

$$\dot{\Phi}(t) = \sum_{k=0}^{N-1} h(k)\Phi(t-k) \quad (2)$$

where $\dot{\Phi}(t)$ is the derivative of the input signal $\Phi(t)$ at time t, and h is the impulse response with order (N-1). Used sequentially, this filter will create a time series of the carrier-phase $\dot{\Phi}(t)$. Applying the same convolution again, one obtains the range accelerations:

$$\ddot{\Phi}(t) = \sum_{k=0}^{N-1} h(k)\dot{\Phi}(t-k) \quad (3)$$

Theoretically, the relationship between the impulse response \mathbf{h} and the ideal digital differentiator is given by:

$$h(nT) = \frac{1}{\omega_s} \int_{-\omega_s/2}^{\omega_s/2} H(e^{j\omega T}) e^{j\omega T} d\omega \quad (4)$$

then, the design of a digital differentiator depends on the choice of the impulse response \mathbf{h} and the order of the filter which is related to the length of the window. Ideally, the order should be chosen in a way that the filter frequency response should respect Eq. (1). On the other hand, when one is interested in generating range rates and range accelerations in real time, the obvious choices are low-order filters.

In our work, the choice was a first order filter, the central difference approximation (first order Taylor series). This filter has the following impulse response:

$$\mathbf{h} = \frac{1}{2} [1 \quad 0 \quad -1]^T \quad (5)$$

which will result in the following differentiator for the carrier-phase rate:

$$\dot{\Phi}(t) \approx \frac{\Phi(t + \Delta t) - \Phi(t - \Delta t)}{2\Delta t} \quad (6)$$

and for the carrier-phase range acceleration:

$$\begin{aligned} \ddot{\Phi}(t - \Delta t) &\approx \frac{\dot{\Phi}(t + \Delta t) - \dot{\Phi}(t - \Delta t)}{2\Delta t} \\ &= \frac{\Phi(t + 2\Delta t) - 2\Phi(t) + \Phi(t - 2\Delta t)}{4\Delta t^2} \end{aligned} \quad (7)$$

The use of the first order central difference approximation of the carrier-phase rate to generate the Doppler observations, as was demonstrated by Szarmes et al. [1997] is easy to implement and provides the most appropriate velocity estimates in low dynamics environments. The same approach can be extended for the accelerations.

The trade-off is that the approximation cannot reflect quite well the receiver dynamics in kinematic situations with unknown dynamics. The first order central difference approximation is a linear prediction of the Doppler shift, which corresponds to a band-pass filter with cut-off frequencies at 0.125 and 0.375 Hz, using 1Hz sampling ($\Delta t = 1s$). The cut-off frequency of the filter is determined at the frequency where the amplitude reaches around 70% (i.e., $1/\sqrt{2}$) of the maximum amplitude.

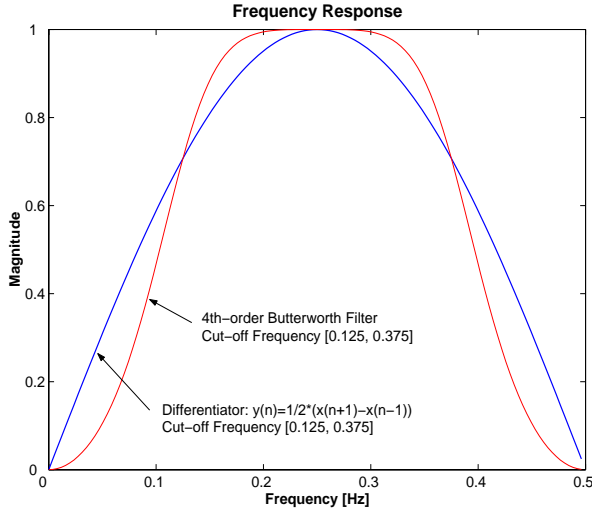


Figure 2: Frequency response of the filter to the amplitude at a 1 Hz sampling rate. The fourth-order Butterworth filter with cut-off frequencies at 0.125 and 0.375 Hz is also plotted in the figure as an example of the conventional, but more complex, band-pass filters which have more or less similar frequency responses.

As is illustrated in Figure 2, the filter of the first order central difference approximation stops the signals at 0 and 0.5 Hz (i.e., Nyquist frequency) for data with 1Hz sampling. At a half of the Nyquist frequency (0.25 Hz), this filter passes the signals without attenuation. Therefore, this filter can perfectly remove constant biases in the signals. However, this filter will reduce the amplitudes of the signals over all frequency components except for a half of the Nyquist frequency. As we carried out the kinematic test at a 1 Hz data rate, the higher-order effects (e.g., all frequency components higher than the Nyquist frequency, 0.5 Hz) of the receiver dynamics will be aliased in the approximation of the carrier phase [Ifeachor and Jervis, 1993].

The first step of our approach is to compute the satellite velocities and accelerations in real time, i.e. from the broadcast ephemeris. Until now, it is not very common to see works on this subject, probably because when one wants acceleration information in real time it is easier to get very precise values (in a short term) from accelerometers, or for other applications, a post-processing procedure using precise ephemerides is adopted. However, proving that satellite velocities and accelerations can be estimated at the order of mm/s and mm/s² respectively, using broadcast ephemerides, it is reasonable to assume that one can also estimate in real time user velocities and accelerations with the same order of accuracy, if the other error sources are properly modeled. The proof comes from solid concepts on satellite dynamics, and the close relationship between the satellite orbital broadcast parameters and their derivatives

in time to obtain not only satellite velocities and acceleration in the orbital plane but also in the Earth-Centred-Earth-Fixed (ECEF) reference frame. The next figures and explanations come from Kennedy [2002] and are very well detailed and explained in that paper.

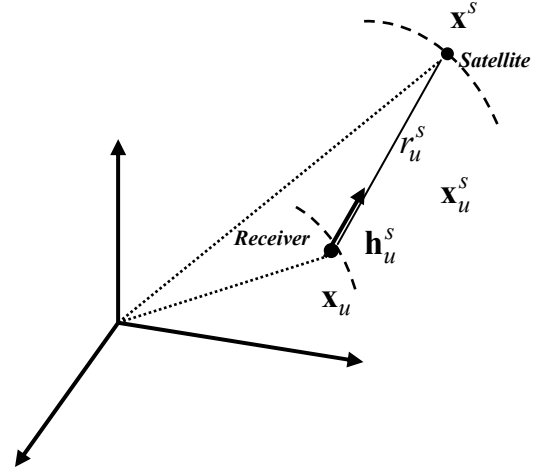


Figure 3: Line-of-sight relative geometry between satellite and user.

$$\mathbf{x}_u^s = \mathbf{h}_u^s r_u^s \quad (8)$$

- \mathbf{x}_u^s is the relative position vector between the user u and the satellite s .
- r_u^s is the geometric range between the user u and the satellite s .
- \mathbf{h}_u^s is the unit direction vector between the user u and the satellite s .

A more useful way of seeing Eq. (8) is putting it in order to the geometric distance:

$$r_u^s = \mathbf{h}_u^s \cdot \mathbf{x}_u^s \quad (9)$$

where differentiating, one obtains the geometric range rate:

$$\dot{r}_u^s = \mathbf{h}_u^s \cdot \dot{\mathbf{x}}_u^s \quad (10)$$

and differentiating two times, one obtain the geometric range acceleration between the user u and the satellite s :

$$\ddot{r}_u^s = \mathbf{h}_u^s \cdot \ddot{\mathbf{x}}_u^s + \dot{\mathbf{h}}_u^s \cdot \dot{\mathbf{x}}_u^s \quad (11)$$

where the first part of Eq. (11) refers to the line-of-sight relative acceleration (which contains the unknown user

acceleration vector), and the second part can be seen as a correction due to the centrifugal acceleration, thus it is a nuisance parameter [Jekeli and Garcia, 1997]. This is illustrated in Fig. 4:

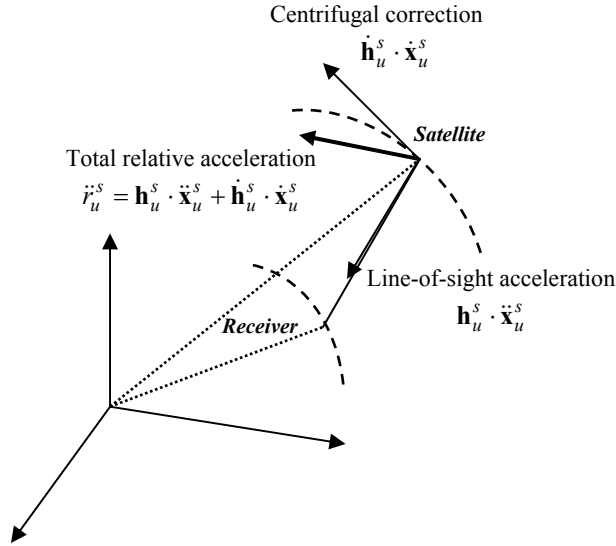


Figure 4: Mechanics of satellite acceleration.

The two quantities, \dot{r}_u^s and \ddot{r}_u^s , are respectively the true geometric range rate and range acceleration, which can be approximated by the difference in time of the carrier-phase, as explained before.

The satellite velocities are obtained through an analytical differentiation in time of the ECEF parameter equations (ICD-GPS-200C):

$$\dot{x}_k = \frac{\delta x_k}{\delta t} \quad \dot{y}_k = \frac{\delta y_k}{\delta t} \quad \dot{z}_k = \frac{\delta z_k}{\delta t} \quad (12)$$

and accelerations:

$$\ddot{x}_k = \frac{\delta^2 x_k}{\delta t^2} \quad \ddot{y}_k = \frac{\delta^2 y_k}{\delta t^2} \quad \ddot{z}_k = \frac{\delta^2 z_k}{\delta t^2} \quad (13)$$

where the ECEF satellite coordinates are:

$$\begin{aligned} x_k &= x'_k \cos \Omega_k - y'_k \cos i_k \sin \Omega_k \\ y_k &= x'_k \sin \Omega_k + y'_k \cos i_k \cos \Omega_k \\ z_k &= y'_k \sin \Omega_k \end{aligned} \quad (14)$$

where x'_k and y'_k are the orbital plane coordinates, i_k is the orbit inclination and Ω_k is the corrected longitude of ascending node. Alternatively, we can convert the orbital plane coordinates to ECEF coordinates by doubly differentiating the expression:

$$\mathbf{x}_u^s = \mathbf{R} \begin{bmatrix} x'_k \\ y'_k \\ 0 \end{bmatrix} \quad (15)$$

where \mathbf{R} is given by:

$$\begin{aligned} \mathbf{R} &= \mathbf{R}_3 \{-\Omega_k\} \mathbf{R}_1 \{-i_k\} \mathbf{R}_3 \{-\omega_k\} = \\ &= \begin{bmatrix} \cos \Omega_k \cos \omega_k - & -\cos \Omega_k \sin \omega_k - & \sin \Omega_k \sin i_k \\ \sin \Omega_k \sin \omega_k \cos i_k & \sin \Omega_k \cos \omega_k \cos i_k & \\ \sin \Omega_k \cos \omega_k + & -\sin \Omega_k \sin \omega_k + & -\cos \Omega_k \sin i_k \\ \cos \Omega_k \sin \omega_k \cos i_k & \cos \Omega_k \cos \omega_k \cos i_k & \\ \sin \omega_k \sin i_k & \cos \omega_k \sin i_k & \cos i_k \end{bmatrix} \end{aligned}$$

to yield:

$$\ddot{\mathbf{x}}_u^s = \begin{pmatrix} \ddot{x}_k \\ \ddot{y}_k \\ \ddot{z}_k \end{pmatrix} = \ddot{\mathbf{R}} \begin{pmatrix} x'_k \\ y'_k \\ 0 \end{pmatrix} + 2\dot{\mathbf{R}} \begin{pmatrix} \frac{\delta x'_k}{\delta t} \\ \frac{\delta y'_k}{\delta t} \\ 0 \end{pmatrix} + \mathbf{R} \begin{pmatrix} \frac{\delta^2 x'_k}{\delta t^2} \\ \frac{\delta^2 y'_k}{\delta t^2} \\ 0 \end{pmatrix} \quad (16)$$

and both methods give identical results.

After the derivation of the satellite velocities and accelerations from the broadcast ephemeris, one can validate them by comparing them with those derived from an NGA (National Geospatial-Intelligence Agency) SP3 file, which contains precise positions and velocities. This can be done using a 9th order Lagrange interpolating polynomial to generate solutions with the rate that best fits our purposes, where n is the polynomial degree:

$$L_j(x) = \prod_{\substack{k=0 \\ k \neq j}}^n \frac{(x - x_k)}{(x_j - x_k)} \quad (17)$$

and the resulting polynomial:

$$P(x) = \sum_{j=0}^n f(x_j) L_j(x) \quad (18)$$

As for the satellite accelerations, since the SP3 file does not contain them, it is easier to use the interpolated velocities and obtain them through numerical differentiation. Our choice was again a first order central difference approximation using a Taylor's expansion:

$$f'(x) = \frac{f(x + \Delta t) - f(x - \Delta t)}{2\Delta t} \quad (19)$$

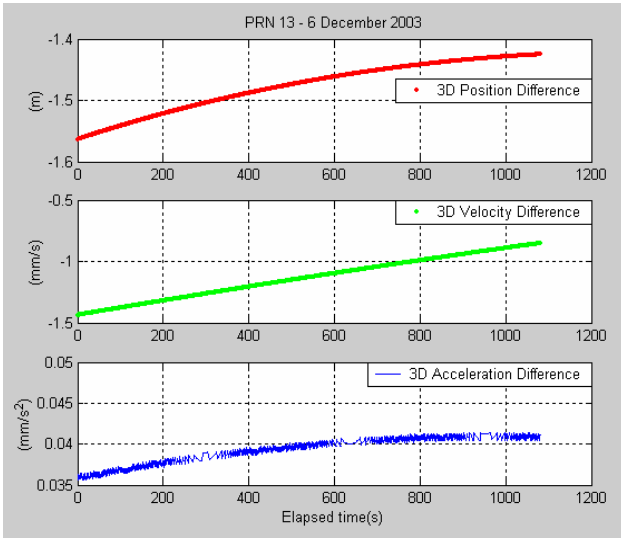


Figure 5: Proof that the satellite velocity and acceleration predicted by using the broadcast ephemeris in the navigation message is sufficiently accurate by comparison to the velocity and derived acceleration of SP3 precise ephemeris.

Before giving the mathematics behind the observables, it is important to understand that although the position solutions are relaxed in the carrier-phase method, their precise determination is nonetheless important to the precise determination of velocity and acceleration. Positioning accuracy of at least 10m is required for the errors caused by the wrong coordinates to be negligible [Itani et al. 2000].

At this point, one is ready to see the relationship between the true geometric range-rate \dot{r}_u^s and the range-rate derived from the carrier-phase differentiation in time $\dot{\Phi}_u^s$. The relationship can be extended for the geometric range acceleration \ddot{r}_u^s and the derived range acceleration $\ddot{\Phi}_u^s$.

Eq. (20) shows the observation equation for the velocity determination.

$$\begin{aligned}\dot{\Phi}_u^s &= \dot{r}_u^s + (\dot{B}_u - \dot{b}^s) + \dot{I}_u^s + \dot{T}_u^s + \delta V^s + \dot{\xi} \\ \dot{\Phi}_u^s &= \dot{r}_u^s + \dot{B}_u + \varepsilon_{u_\phi}^s\end{aligned}\quad (20)$$

where \dot{r}_u^s stands for the geometric range rate between the receiver u and satellite s ; \dot{B}_u for the receiver clock drift; \dot{b}^s for the satellite clock drift; \dot{I}_u^s for the ionospheric delay rate; \dot{T}_u^s for the tropospheric delay rate, δV^s the error in satellite velocity derivation and $\dot{\xi}$ for the receiver system noise.

Similarly, the equation for the range acceleration is:

$$\begin{aligned}\ddot{\Phi}_u^s &= \ddot{r}_u^s + (\ddot{B}_u - \ddot{b}^s) + \ddot{I}_u^s + \ddot{T}_u^s + \delta A^s + \ddot{\xi} \\ \ddot{\Phi}_u^s &= \ddot{r}_u^s + \ddot{B}_u + \varepsilon_{u_\phi}^s\end{aligned}\quad (21)$$

with all the modeled quantities in the equation behaving as second order errors (for instance, \ddot{B}_u is the receiver clock drift rate) and δA^s is the error in the satellite acceleration calculation.

Since we use the pseudorange measurements for the position solutions and the carrier-phase for deriving range rates and range accelerations, we can model out some of the errors in the raw observations. They are the errors in satellite clock, propagation effects in the ionosphere and troposphere, and receiver system noise, which can be summarised as in Eqs. (22), though at this point they refer already to the first and second order (rate) effects:

$$\begin{aligned}\varepsilon_{u_\phi}^s &= -\dot{b}^s + \dot{I}_u^s + \dot{T}_u^s + \delta V^s + \dot{\xi} \\ \varepsilon_{u_\phi}^s &= -\ddot{b}^s + \ddot{I}_u^s + \ddot{T}_u^s + \delta A^s + \ddot{\xi}\end{aligned}\quad (22)$$

The effects of satellite clock bias and drift were modeled out using the coefficients in the navigation message [ICD-GPS-200, 1999]. The relativistic effect and group delay differential are also accounted for using appropriate algorithms with values given in the navigation message. To reduce the effect of the tropospheric delay in the measurements, we use the UNB3 tropospheric prediction model [Collins and Langley, 1997], which is based on the zenith delay algorithms of Saastamoinen [1973], the mapping functions of Niell [1996], and a table of sea-level atmospheric values derived from the U.S. 1966 Standard Atmosphere Supplements, and lapse rates to scale the sea-level values to the receiver height. For reducing the effects of ionospheric delay, we use the standard (Klobuchar) model using the parameter values in the navigation message. Since we use the time-differenced measurements over a short time interval (that is, less than or equal to 2 seconds) for velocity and acceleration determination, the residual effects of the tropospheric and ionospheric delays, if any, are normally negligible.

After modeling the measurements accordingly, the observation equations for velocity and acceleration are now given by:

$$\dot{\Phi}_u^s = \mathbf{h}_u^s \cdot (\mathbf{v}_u - \mathbf{V}^s) + \dot{B}_u + \varepsilon_{u_\phi}^s \quad (23)$$

$$\ddot{\Phi}_u^s = \dot{\mathbf{h}}_u^s \cdot (\mathbf{v}_u - \mathbf{V}^s) + \mathbf{h}_u^s \cdot (\mathbf{a}_u - \mathbf{A}^s) + \ddot{B}_u + \varepsilon_{u_\phi}^s \quad (24)$$

where one can see explicitly the relation between the derived observations through differentiation, and those from Eqs. (10) and (11), \mathbf{V}^s and \mathbf{A}^s stand for the satellite velocity and acceleration vectors; \mathbf{v}_u and \mathbf{a}_u for the receiver velocity and acceleration vectors; and \mathbf{h}_u^s represents the directional cosine vector between the receiver and satellite.

We can describe the estimates of the unknown parameters for both the velocity and acceleration, in the least-squares sense:

$$\mathbf{x}_v = [v_x \ v_y \ v_z \ \dot{B}_u]^T \quad \text{and} \quad \mathbf{x}_a = [a_x \ a_y \ a_z \ \ddot{B}_u]^T$$

The formulation of the stochastic model \mathbf{Q} for velocity and acceleration determination is based on the assumption that the relationship between satellite elevation angle and system noise can be quite well modeled by an exponential function [Jin, 1996]. Since most of the biases and errors in the measurements will be cancelled in the first order central difference approximation of the carrier-phase rate, such an assumption can be easily justified.

Assuming no temporal correlation in the carrier phase observations and no correlation among the receiver channels, we will have (an example just for the range rate, but the same reasoning can be applied for the range acceleration):

$$\mathbf{Q}_{\Phi_k^j} = \begin{bmatrix} \sigma_{\Phi_k^j}^2 & & & \\ & \sigma_{\Phi_k^j}^2 & & \\ & & \ddots & \\ & & & \sigma_{\Phi_k^j}^2 \end{bmatrix}, \quad (25)$$

where

$$\sigma_{\Phi_k^j}^2 = \frac{1}{4 \cdot \Delta t^2} \left(\sigma_{\Phi_{k+M}^j}^2 + \sigma_{\Phi_{k-M}^j}^2 \right). \quad (26)$$

Furthermore, the variance of the first order central difference approximation of the carrier-phase rate was fitted to the exponential function as:

$$\sigma_{\Phi_k^j}^2 = a_0 + a_1 \exp\left(\frac{a_2}{ELEV_k^j}\right), \quad (27)$$

where $ELEV$ represents the elevation angle of the satellite. In order to model the system noise, we need to estimate correctly the coefficients a_0 , a_1 and a_2 in Equation (27). The first two coefficients are expressed in $(\text{m/s})^2$ and the third one is in degrees, where they can be estimated by means of least-squares estimation.

TESTS PERFORMED

After the implementation of the algorithms for real-time velocity and acceleration, we performed some practical tests, both static and kinematic. Obviously the real-time kinematic accelerations were our first goal, though we also wanted to evaluate the performance of the algorithms using a low-cost single-frequency GPS receiver with a patch antenna (Furuno GS-77), in a medium to high multipath environment (Fig. 6).



Figure 6: Components of the low-cost GPS receiver used in the static test, in a multipath environment.

The acceleration results from the static test (Fig. 7) were at the millimeter/s² level, and as expected the only feature present is amplified noise due to the differentiation process, since the only dynamics involved were the satellite velocity and acceleration.

Table 1: Static acceleration statistics.

mm/s ²	Mean	Std	Rms
East	0.1	1.0	1.0
North	0.6	1.3	1.4
Up	-0.8	2.4	2.5

The GNSS-derived acceleration only reflects the user kinematic acceleration, thus the gravity acceleration is not present as one can see from the bottom panel in Fig. 7.

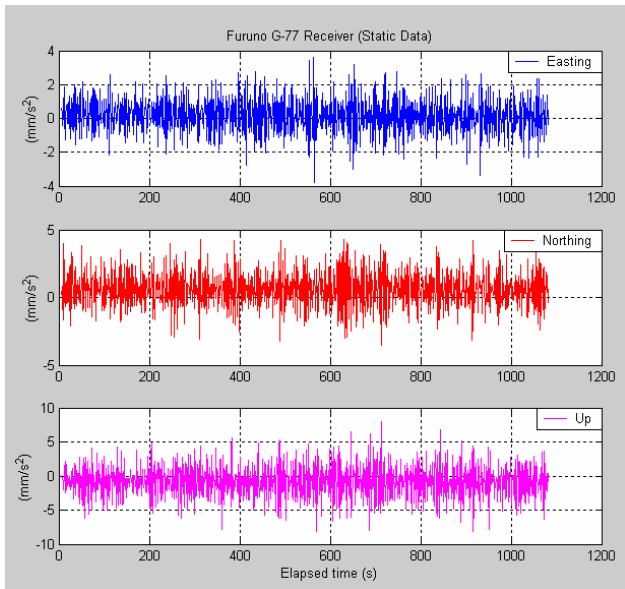


Figure 7: Results from the static acceleration test, giving the east, north and up components.

The residuals also show that the functional model performed quite well for the static test, though there is a remaining bias in the residuals for some satellites, especially those with very low elevation angle (no elevation cut off angle was used for the test), which highlights the fact that better stochastic models should be evaluated.

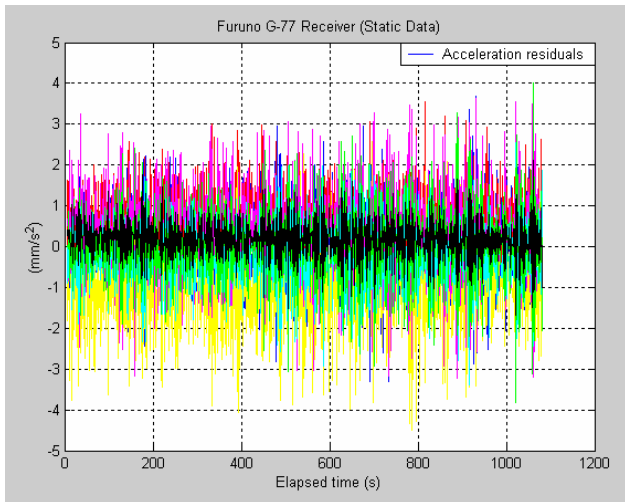


Figure 8: Phase acceleration residuals from the least-squares estimation of static acceleration.

After the static test, we performed a kinematic one, using a NovAtel OEM4 receiver, with a pinwheel antenna GPS-600, mounted on the top of a vehicle (Fig. 9). The data was collected at a 10 Hz rate, though the algorithms at this stage are developed for 1 Hz rate processing and so the data was decimated to 1Hz.



Figure 9: Setup of a NovAtel antenna on the top of the vehicle, for the kinematic test.

The test was performed on a highway surrounding the city of Fredericton and its accesses, where it is possible to use higher velocities, higher accelerations or decelerations, thus providing experience of different dynamics. We collected 1 hour's data, though we chose to process 15 minutes, where there are good RTK (real-time kinematic) solutions to validate the velocities and acceleration results. Figure 10 depicts the area covered during those 15 minutes.

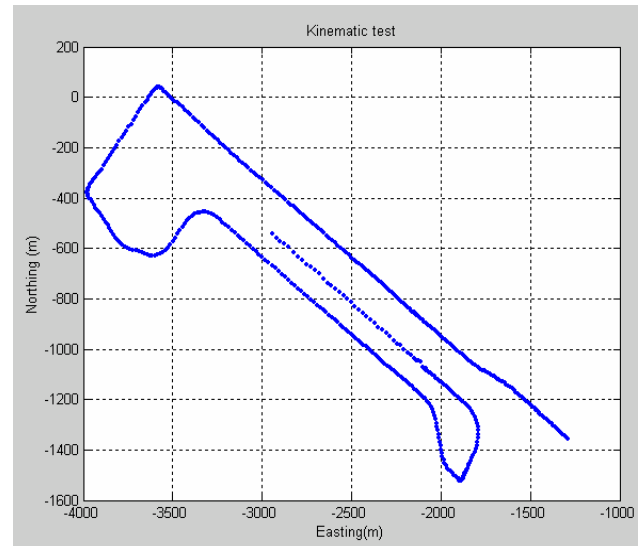


Figure 10: Area covered during the kinematic test with RTK solutions for validation purposes.

As one can see from Fig. 11, the vehicle experienced a range of dynamics, showing some stops, idling, accelerating or fast decelerating.

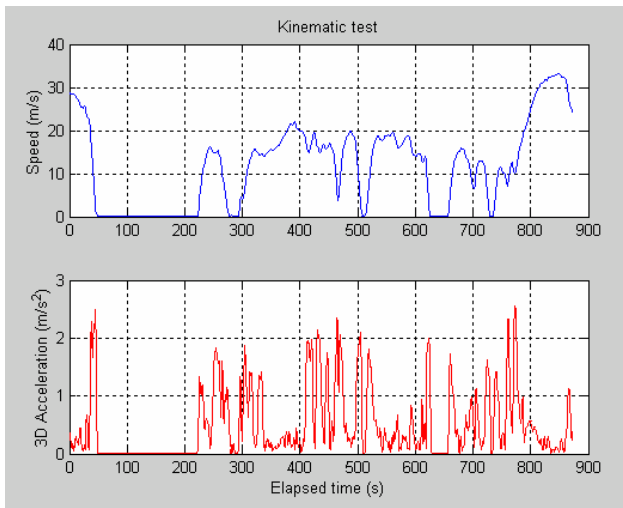


Figure 11: The 3D speed and 3D acceleration under different dynamics during the kinematic test.

The next figure shows the velocity components in the local level system (LLS), also known as the ENU system.

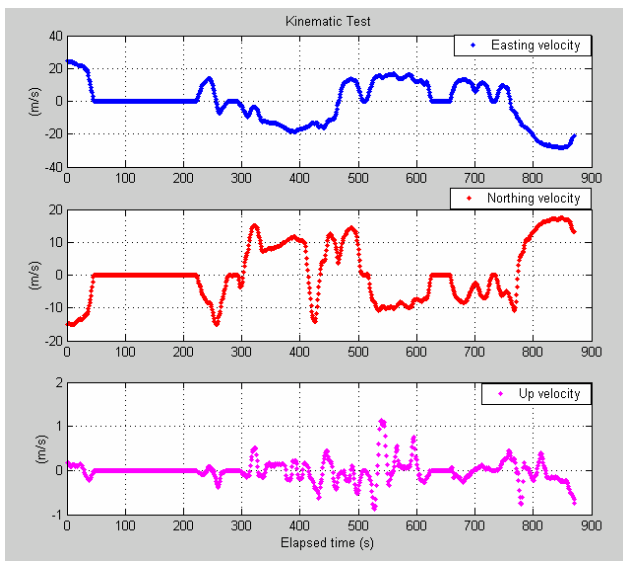


Figure 12: East, north and up velocity components during the kinematic test.

The next figure (Fig. 13) shows the acceleration components also in the ENU system. We can easily identify the different dynamics situations from both the velocity and acceleration figures, for instance during the moments when the car was stopped or when it was accelerating, and respective velocity and acceleration responses.

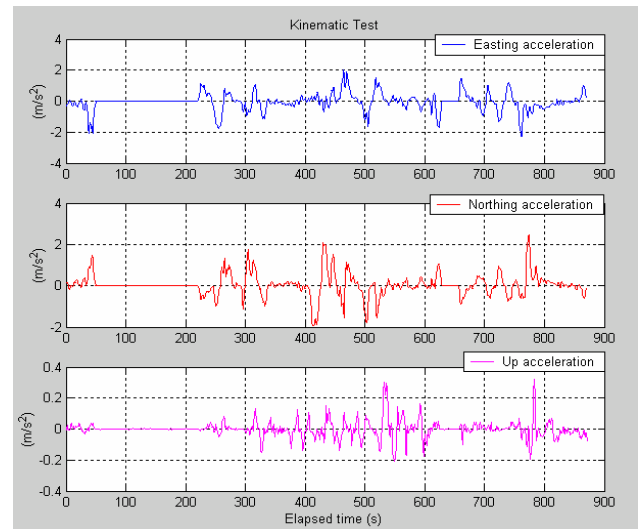


Figure 13: East, north and up acceleration components during the kinematic test.

In a static test, it is easy to validate the estimates by comparing the velocities and accelerations with the zero truth values, whereas in a kinematic test the task becomes more complex. In our case, the option was to use the RTK precise positions using the UNB RTK system, which gives position solutions better than 2cm at 2-sigma value [Kim and Langley, 2003], and derive the velocities and accelerations through numerical differentiation of the positions. Fig. 14 shows the difference between the “reference” velocity values coming from the RTK-derived velocities and those derived from the single-receiver measurements. Hence, for our purposes they represent the velocity errors in the carrier-phase differencing method.

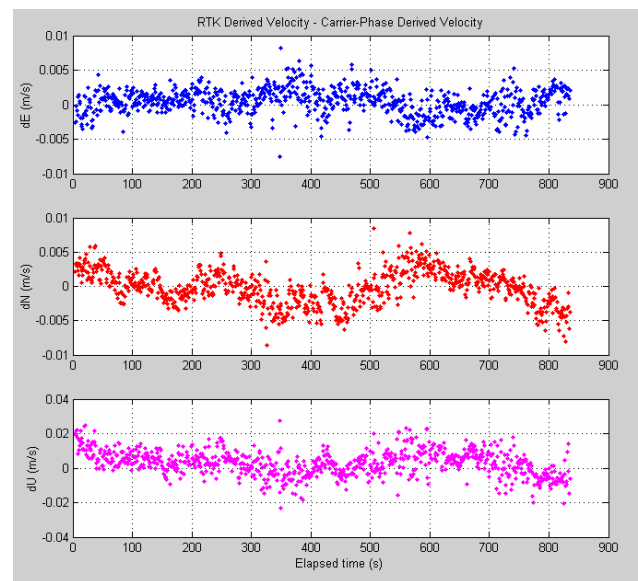


Figure 14: Difference between the RTK derived velocities and those derived from the carrier-phase method.

Table 2: Velocity statistics in the three LLS components. Note that 5 mm/s is approximately 0.02 km/h.

mm/s	Mean	Std	Rms
East	0	1.8	1.8
North	0	2.4	2.4
Up	2.9	7.4	7.9

For the acceleration, it was analyzed using exactly the same procedure, i.e., derive what we consider the “truth” accelerations from the RTK solutions and compare them with those derived from the carrier-phase method.

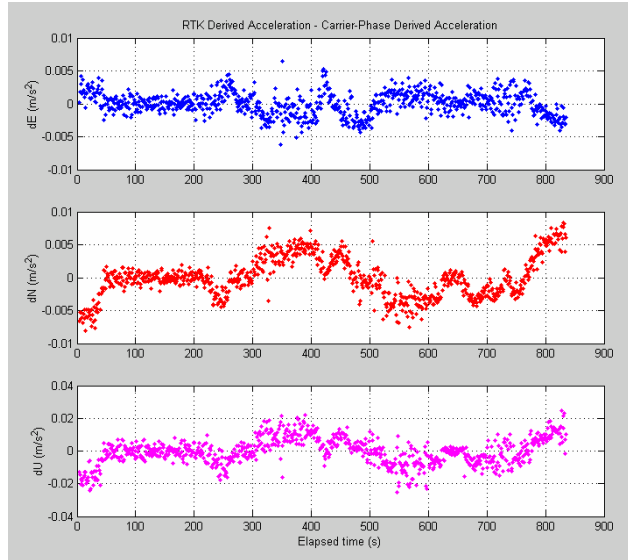


Figure 15: Difference between the RTK derived accelerations and those derived from the carrier-phase method.

Overall the results are at the mm/s² level, as described in Table 3, which may be considered promising at this preliminary stage, though many other kinematic tests should be performed.

Table 3: Acceleration statistics in the three LLS components.

mm/s ²	Mean	Std	Rms
East	0	1.7	1.7
North	0	3.1	3.1
Up	0	8.1	8.1

It is interesting to note that when the car was stopped, the errors are quite small and not biased, exactly as noted in the static test, but when the car experiences higher dynamics, not only is the scatter in the errors magnified but the results become biased, which can also be seen in the residuals (Fig. 16, bottom panel).

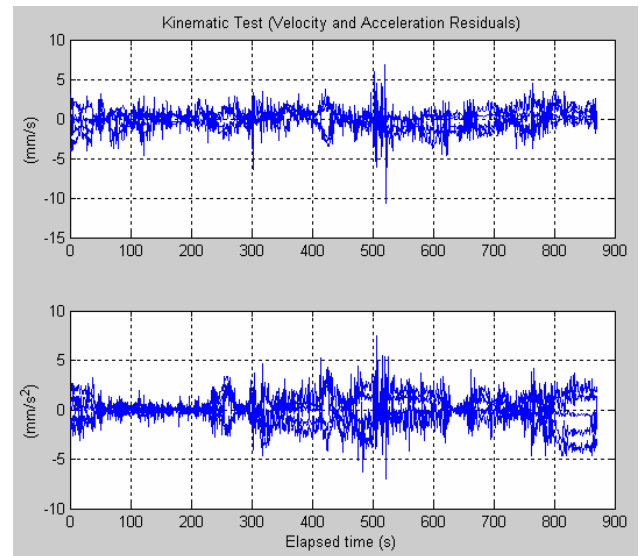


Figure 16: Velocity and acceleration residuals from the kinematic test.

This might come from the fact that as we carried out the kinematic test at a 1 Hz data rate, the higher-order effects (e.g., all frequency components higher than the Nyquist frequency, 0.5 Hz) of the receiver dynamics will be aliased in the approximation of the carrier phase [Ifeachor and Jervis, 1993]. Besides, the numerical differentiation of the RTK position solutions eliminate some errors but amplifies the noise in some bandwidths, thus these derived velocities and accelerations can not be considered as absolute truth. Hence, the plots in Fig. 14 and 15 may be giving a too pessimistic idea of the performance of the technique.

Since these preliminary results are promising, why not use this important dynamic information gathered in real time, and fed into a Kalman filter, together with the pseudoranges to improve the positions in the solution domain?

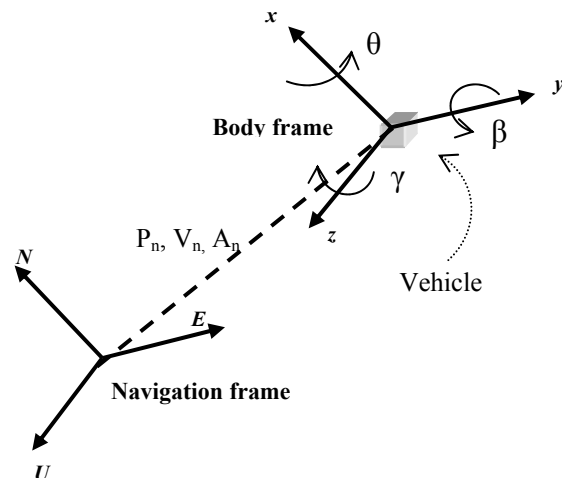


Figure 17: Relation between the navigation frame and the body frame, with dynamics involved.

Looking at Fig. 17, one can see the advantages of having acceleration information already in the navigation frame, thus being able to augment the system and improve the position estimates, as in a GPS/INS system. The limitation in this case is the fact that the range rates and range accelerations are themselves correlated in time and cross-correlated between them, thus it is not a good approach to use them as in a tightly-coupled Kalman filter. This can be seen in the acceleration residuals spectrum (Fig. 18).

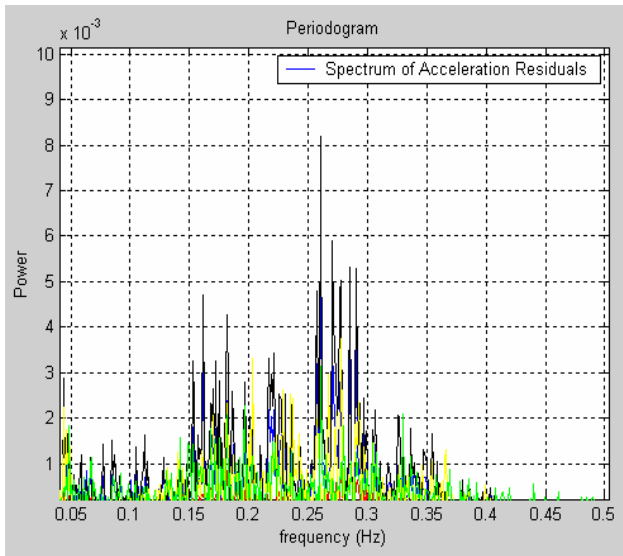


Figure 18: Periodogram (spectrum) of the acceleration residuals.

Using “whitening” filters can be a good option, though this procedure should be used with caution since the transformation can change the original range rates and accelerations into a “white” subspace, which is not exactly the same as the original and may mask the dynamics. Another option, which we have chosen, is using the velocity and acceleration in the solution domain as if they were coming from real speedometers and accelerometers. This is implemented through an extended Kalman filter (EKF).

The nonlinear dynamical model is described by:

$$\mathbf{x}_k = f(\mathbf{x}_{k-1}, k-1) + \mathbf{w}_{k-1} \quad (29)$$

$$\mathbf{w}_k \sim N(0, \mathbf{Q}_k)$$

where the state vector is given by:

$$\mathbf{x}_k = [\mathbf{p}, \mathbf{v}, \mathbf{a}, \mathbf{dt}]$$

$$\mathbf{p} = (x, y, z)$$

$$\mathbf{v} = (v_x, v_y, v_z)$$

$$\mathbf{a} = (a_x, a_y, a_z)$$

$$\mathbf{dt} = (dt, d\dot{t}, d\ddot{t})$$

The nonlinear measurement model is:

$$\mathbf{z}_k = h(\mathbf{x}_k, k) + \mathbf{v}_k \quad (30)$$

$$\mathbf{v}_k \sim N(0, \mathbf{R}_k)$$

where the measurements are the differences between the observed pseudoranges and the predicted ones, the estimated velocities, accelerations, receiver clock drift and drift rate.

$$\mathbf{z}_k = [\delta P_1, \dots, \delta P_m, \hat{v}_x, \hat{v}_y, \hat{v}_z]$$

$$\hat{\mathbf{v}} = (\hat{v}_x, \hat{v}_y, \hat{v}_z)$$

$$\hat{\mathbf{a}} = (\hat{a}_x, \hat{a}_y, \hat{a}_z)$$

$$\hat{\mathbf{dt}} = (\hat{dt}, \hat{d\dot{t}})$$

and, assuming no correlations between them, the covariance is given by the values derived from the overall precision in the study performed in the previous section. For the pseudoranges, reference values for the receiver (accuracy of single point L1 $\sigma_{L1}^2 \approx 4m^2$) were used.

$$\mathbf{R}_k = \begin{bmatrix} \mathbf{R}_{\sigma_{\delta P}} & 0 & 0 & 0 \\ 0 & \mathbf{R}_{\sigma_{\hat{v}}} & \vdots & \vdots \\ \vdots & \vdots & \mathbf{R}_{\sigma_{\hat{a}}} & \vdots \\ 0 & 0 & 0 & \mathbf{R}_{\sigma_{\hat{dt}}} \end{bmatrix}$$

The predicted state estimate was computed as:

$$\hat{\mathbf{x}}_k^{(-)} \approx f(\hat{\mathbf{x}}_{k-1}^{(+)}, k-1) \quad (31)$$

and the linear approximation equations give:

$$\Phi_{k-1} \approx \left. \frac{\partial f(\mathbf{x}, k-1)}{\partial \mathbf{x}} \right|_{\mathbf{x}=\hat{\mathbf{x}}_{k-1}^{(-)}}$$

$$= \begin{bmatrix} 1 & \Delta t & \frac{\Delta t^2}{2} & 0 \\ 0 & 1 & \Delta t & 0 \\ 0 & 0 & 1 & 0 \\ 0 & 1 & \Delta t & \frac{\Delta t^2}{2} \end{bmatrix} \quad (32)$$

The next figure depicts the results, i.e., the difference from the Kalman filter position results (implemented with

the velocities and accelerations coming from the carrier-phase method) and the positions from the RTK solutions. Thus, it reflects the errors in this new approach for improving positions using GNSS-derived accelerations.

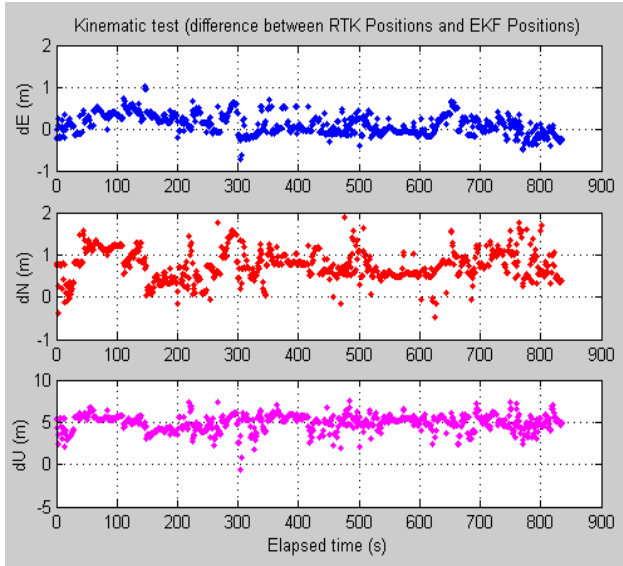


Figure 19: Difference between the RTK solutions and the position solutions from the EKF implementation.

Looking at the figure, it is very clear that the position estimates are improved by one order of magnitude, since a regular point position algorithm in real time typically provides 3D solutions with a precision around 10 m and, at best, a few metres. Here, we see an overall precision around 1m:

$$\sigma_E = 0.23m \quad \sigma_N = 0.35m \quad \sigma_U = 0.95m$$

In addition, the residuals show a small spread, around ± 2 m, though they also clearly show that some residual constant biases remain.

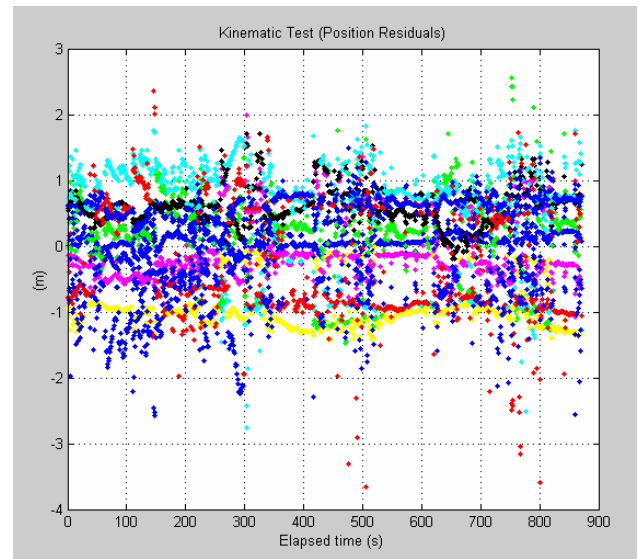


Figure 20: Residuals from the EKF position solutions.

This is due in part, to the fact that we are only using the L1 pseudorange to derive the position, and though the atmospheric errors are modeled using the Klobuchar model for the ionospheric delay prediction and the UNB3 model for the tropospheric delay prediction, residual errors remain.

CONCLUDING REMARKS

A standalone GPS receiver can be used to obtain horizontal velocities at the few mm/s level, and horizontal accelerations at the few mm/s² level, in real-time kinematic scenarios. The corresponding vertical values are a factor of 2-3 worse. The static acceleration results show even better rms values, especially in the up component where this value is three times better (2.5 mm/s²) than the up kinematic acceleration. Some of the reported “errors” could be due to the errors in the RTK “truth” values.

The carrier-phase method to derive velocities and accelerations is accurate enough for many real time kinematic applications, and at the same time is a simple, easy to operate and cost-effective technique, thus becoming a very attractive option.

Although the overall goal for this paper was not the study of any precise point positioning technique (PPP), it became clear that the input of available dynamic information (already in the navigation frame), i.e the estimated velocities and accelerations could actually augment the system, hence filter and improve the position solutions, becoming an interesting PPP technique.

FURTHER RESEARCH

Based on the concluding remarks, it is worth considering the implementation of higher order filters or optimal ones based on higher dynamics, using up to 50 Hz GPS data. This can circumvent two problems, which are the dynamics aliasing created in the differentiation process, and the unrealistic dynamics picture taken using only 1s samples (1 Hz). Besides, the use of very high GNSS data rates can also overcome the problem of time latency between the position, velocity and acceleration results.

The development of higher order filters for higher dynamics thus requires the improvement of the functional model for the new dynamics, also extending the study for different platforms. This can be done with the aid of a GPS hardware simulator, easily generating GPS data in a myriad of different dynamics scenarios. The use of a precise motion table can also help to understand the correct velocity and acceleration frequency components from a specific signal, thus making easier the design of the filter for a specific bandwidth. On the other hand, if one is developing functional models for unknown or higher dynamics, it is also desirable to implement new stochastic models, such as adaptive ones, which can more realistically reflect the change in the measurements quality, affected by the change in the receiver dynamics.

At this point, it is obvious that one should study the integration of GNSS-derived velocity and acceleration with those coming from inertial navigation systems. This can provide a way to help mitigate the predominant error sources in the inertial sensors, such as bias, scale factors or random walk. On the other hand, the outputs from the inertial sensors can provide the dynamic information in situations where the GNSS-derived velocity and accelerations are not available due to the blockage of the LOS (line-of-sight) between satellite and receiver.

The improvement of the PPP technique using the GNSS-derived velocity and acceleration should be accompanied with the integration of better error models. This means that in order to fully evaluate the inherent improvement in position due to the integration of GNSS derived velocity and acceleration, it is also necessary to carry out better modeling so that we can take care of all sources of errors and biases.

ACKNOWLEDGMENTS

The work described in this paper was supported by the Natural Sciences and Engineering Research Council of Canada.

REFERENCES

- A. M. Bruton, C. L. Glennie and K. P. Schwarz (1999). "Differentiation for High-Precision GPS Velocity and Acceleration Determination." *GPS Solutions*, Vol. 2, No. 4, pp. 4-21.
- Collins, J.P. and R.B. Langley (1997). "Estimating the Residual Tropospheric Delay for Airborne Differential GPS Positioning." Proceedings of the 10th International Technical Meeting of the Satellite Division of The Institute of Navigation, Kansas City, Missouri, 16-19 September, pp. 1197-1206.
- ICD-GPS-200C (1999). *Navstar GPS Space Segment/Navigation User Interface Control Document*, GPS Navstar JPO, 138 pp.
- Ifeachor, E. C. and B. W. Jervis (1993). *Digital Signal Processing: A Practical Approach*. Addison-Wesley Publishing Co., Workingham, England.
- Itani, K., T. Hayashi and M. Ueno (2000). "Low-Cost Wave Sensor Using Time Differential Carrier Phase Observations." Proceedings of ION GPS 2000, Salt Lake City, Utah, 19-22 September, pp. 1467-1475.
- Jekeli, C. and R. Garcia (1997). "GPS Phase Accelerations for Moving-base Vector Gravimetry." *Journal of Geodesy*, Vol. 71, No. 10, pp. 630-639.
- Jin, X. (1996). *Theory of Carrier Adjusted DGPS Positioning Approach and Some Experimental Results*. Delft University Press, Delft, The Netherlands, 162 pp.
- Kaplan, E.D. (Ed.) (1996). *Understanding GPS, Principles and Applications*, Artech House Publishers, Boston-London, 554 pp.
- Kennedy, S. (2002). "Precise Acceleration Determination from Carrier Phase Measurements." Proceedings of ION GPS 2002, Portland, Oregon, 24-27 September 2002, pp. 962-972.
- Kim, D. and R.B. Langley (2003). "On Ultrahigh-Precision Positioning and Navigation." *Navigation: Journal of The Institute of Navigation*, Vol. 50, No. 2, Summer, pp. 103-116.
- Misra, P. and P. Enge (2001), *Global Positioning System: Signals, Measurements, and Performance*. Ganga-Jamuna Press, Lincoln, Massachusetts, 390 pp.
- Niell, A.E. (1996). "Global Mapping Functions for the Atmosphere Delay at Radio Wavelengths." *Journal of*

Geophysical Research, Vol. 101, No. B2, pp. 3227-3246.

- Ryan, S., G. Lachapelle and M. E. Cannon (1997). "DGPS Kinematic Carrier Phase Signal Simulation Analysis in the Velocity Domain." Proceedings of ION GPS 97, Kansas City, Missouri, 16-19 September 1997, pp. 1035-1045.
- Serrano, L., D. Kim, and R. B. Langley (2004). "A GPS Velocity Sensor: How Accurate Can It Be? – A First Look." Proceedings of NTM 2004, the 2004 National Technical Meeting of The Institute of Navigation, San Diego, CA, 26-28 January 2004; pp. 875-885.
- Szarmes, M., S. Ryan, G. Lachapelle and P. Fenton (1997). "DGPS High Accuracy Velocity Determination Using Doppler Measurements", Proceedings of KIS 97, Department of Geomatics Engineering, The University of Calgary, Banff, 3-6 June 1997, pp. 167-174.
- Van Graas, F. and A. Soloviev (2003). "Precise Velocity Estimation Using a Stand-Alone GPS Receiver." Proceedings of ION NTM 2003, Anaheim, California, 22-24 January 2003, pp. 262-271.
- Zhang J., K. Zhang, R. Grenfell and R. Deakin (2003). "Realtime GPS Orbital Velocity and Acceleration Determination in ECEF System." Proceedings of ION GPS/GNSS 2003, Portland, Oregon, 9-12 September 2003; pp. 1288-1296.